



# Spectroscopic ellipsometry of very rough surfaces

SUBIAO BIAN<sup>1,2,3</sup> AND ORIOL ARTEAGA<sup>2,3,\*</sup> 

<sup>1</sup>National and Local Joint Engineering Research Center for Intelligent Manufacturing Technology of Brittle Material Products, Huaqiao University, Xiamen 361021, China

<sup>2</sup>Dep. Física Aplicada, PLAT Group, Universitat de Barcelona, Barcelona 08028, Spain

<sup>3</sup>Institute of Nanoscience and Nanotechnology (IN2UB), Universitat de Barcelona, Barcelona 08028, Spain  
\*oarteaga@ub.edu

**Abstract:** This work expands the use of spectroscopic ellipsometry to surfaces with roughness that is similar to or larger than the wavelength of the incident light. By using a custom-built spectroscopic ellipsometer and varying the angle of incidence, we were able to differentiate between the diffusely scattered and specularly reflected components. Our findings demonstrate that measuring the diffuse component at specular angles is highly beneficial for ellipsometry analysis, as its response is equivalent to that of a smooth material. This allows for accurate determination of the optical constants in materials with extremely rough surfaces. Our results have the potential to broaden the scope and utility of the spectroscopic ellipsometry technique.

© 2023 Optica Publishing Group under the terms of the [Optica Open Access Publishing Agreement](#)

## 1. Introduction

Ellipsometry is a powerful technique that utilizes the Fresnel equations to calculate the complex refractive index of a surface from the change in the polarization state of reflected light. Fresnel equations are derived from Maxwell's equations and assume a perfectly smooth surface. However, in reality, surfaces are rarely smooth, and even small variations in surface roughness can significantly affect the measured optical properties. To address this issue, various ellipsometry models [1,2] have been developed over the past decades to analyze surfaces with small random roughness whose characteristic length is much smaller than the wavelength of the incident light. One such example is the effective medium approximation (EMA) theory model [3–6], which treats a slightly rough surface as an equivalent smooth overlayer film, with a refractive index that is the average of the material and the immersion medium.

Interestingly, research in ellipsometry has largely overlooked situations where the characteristic length scale of roughness is comparable to or larger than the wavelength of the incident light. This is likely due to the fact that when roughness is significant, the specularly reflected beam can be partially or completely destroyed, as the incident light is scattered in many directions, resulting in a much weaker intensity of light in the specular direction than in the case of smooth or small roughness surfaces. In such conditions, ellipsometry measurements may be difficult or even impossible with conventional ellipsometers, which are not typically designed to work with low light levels. However, aside from these technical challenges, there is no fundamental reason to exclude very rough surfaces from ellipsometry analysis. Expanding ellipsometry to include these types of surfaces can be highly valuable as natural surfaces and certain soft materials often exhibit very rough surfaces that do not specularly reflect light and cannot be easily polished or processed to create smooth surfaces.

Scattering of light on rough surfaces is a well-studied topic in physics, approached from a variety of analytical and numerical perspectives due to its diverse range of applications, including remote sensing, oceanography, communications, computer graphics, and material science. Recently, this problem has been frequently described in terms of a bidirectional reflectance distribution function (BRDF), which defines how light is reflected from opaque surfaces [7]. Studies have

also been conducted on polarization or polarimetric BDRF, often using Mueller matrices to express the results [8–10]. However, to our knowledge, these studies have not yet had a significant impact on the application of ellipsometry in material science. In general, ellipsometry of very rough surfaces can be considered a specific case of more general polarimetric scattering theories [11,12], where detection is made at a specular angle relative to the incidence and the light source is spectroscopic.

In ellipsometry, as well as other optical techniques, the concept of roughness encompasses not only the topographical properties of a surface but also the conditions of light-matter interaction during measurement. As a result, under certain conditions, a rough surface can be considered "effectively" smooth as it reflects light specularly. More than a century ago, Rayleigh proposed a roughness criterion [13], similar to the well-known angular resolution criterion, to quantitatively determine the conditions under which specular reflection can occur from a rough surface. This criterion highlights that the specular reflection of light depends not only on the size of roughness but also on the incident angle and wavelength, which are parameters that can be controlled in ellipsometry measurements.

This study presents our findings on the characterization of extremely rough surfaces using spectroscopic ellipsometry. We were able to achieve this by using a Mueller matrix ellipsometer that utilizes long integration times to detect the low-intensity light scattered by a very rough surface at the specular angle. By implementing a discrete rotation pattern for the compensator, we were able to independently control the integration time at the detector, making our measurements possible, even when only diffuse light could be observed. Our method contrasts with the traditional continuously rotating setups, which limit the exposure time for each intensity acquisition. To better understand the impact of the Rayleigh roughness criterion on ellipsometry results, we conducted Mueller matrix measurements at various angles of incidence and wavelengths on rough samples of silicon and silver, and developed a simple model to interpret and analyze our results. Contrarily to what one might expect, our results indicate that ellipsometry measurements on very rough surfaces can sometimes be easier to analyze than measurements on surfaces with small roughness, enabling the measurement of optical constants of materials with surfaces that were previously considered unsuitable for ellipsometry measurements.

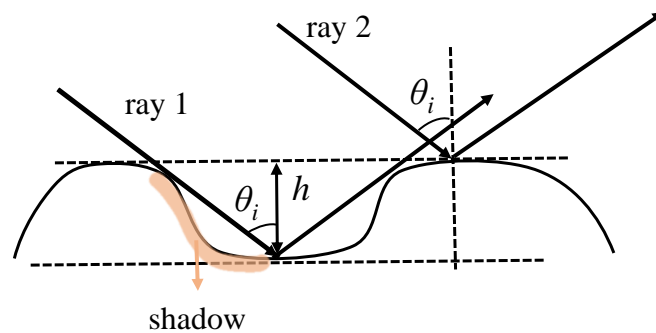


**Fig. 1.** Phase difference of the reflected wave between ray 1 and ray 2, owing to the surface roughness. The part of the surface that can not be illuminated is a shadowed region.

## 2. Theoretical description

We consider light reflection on a randomly rough surface. Following the description in [14,15], we denote the total reflected field resulting from the contribution of all reflected fields from the random heights of the surface as  $E_r$ .  $E_r$  can be split into two contributions:

$$E_r = \langle E_r \rangle + \delta E_r, \quad (1)$$

where  $\langle E_r \rangle$  is the field's mean component and  $\delta E_r$  is the fluctuating component. The angular brackets  $\langle \dots \rangle$  denote a statistical average.  $\langle E_r \rangle$  is found around the specular direction of reflection and can be considered a coherent component due to its well-defined phase relation with the incident wave. On the other hand,  $\delta E_r$  is generated by roughness and represents the incoherent (or diffuse) fields that show angular spreading and weak correlation with the incident wave. The statistical average of the diffuse fields is zero ( $\langle \delta E_r \rangle = 0$ ).

The total reflected intensity by the rough surface can be written as

$$\langle |E_r|^2 \rangle = |\langle E_r \rangle|^2 + \langle |\delta E_r|^2 \rangle. \quad (2)$$

For a perfectly flat surface, the incoherent term  $\langle |\delta E_r|^2 \rangle$  vanishes and  $|\langle E_r \rangle|^2$  is maximum. However, as the surface roughness increases, the coherent term is damped and can become very weak or effectively disappear. From an electromagnetic perspective, the roughness of a surface is influenced not only by the height of the surface, but also by the frequency and angle of the incident wave. This means that a single surface can be perceived as rough or smooth depending on the conditions of the measurement. This is because the impact of roughness on the electromagnetic response is linked to the phase variations  $\delta\phi_r$  of the reflected waves relative to its mean value, which corresponds to the phase of an "equivalent" flat surface. Figure 1 shows an illustrative example of the phase difference between two reflected rays produced by surface roughness.

Under the tangent plane approximation (sometimes called Kirchhoff approximation or Beckmann-Kirchhoff approximation [16]) that is valid for large surface curvature radius and gentle slopes the effect of roughness in the coherent scattered field can be expressed as

$$\langle E_r \rangle = E_0 \langle \exp(i\delta\phi_r) \rangle. \quad (3)$$

The phase variation  $\delta\phi_r$  at a given point of the surface for the coherent scattered field can be written as

$$\delta\phi_r = 2\delta h_A \frac{2\pi}{\lambda} \cos \theta_i, \quad (4)$$

where  $\theta_i$  is the angle of incidence (AOI) with respect to the surface normal  $\lambda$  is the wavelength of light and  $\delta h_A$  is the height variation with respect to the mean value ( $\delta h_A = h_A - \langle h_A \rangle$ ) at a given point of the surface. The Rayleigh roughness criterion states that if the phase variation is very small ( $\delta\phi_r \ll \frac{\pi}{2}$ ) for all points of the surface then all reflected waves are nearly in phase and will interfere constructively and the surface will reflect light specularly, like if it was a perfectly flat surface [17]. This happens not only when the height variation ( $\delta h_A$ ) is very small but also when the AOI approaches grazing incidence ( $\theta_i \rightarrow 90^\circ$ ) even if the roughness is large. However, when there is a non-negligible phase variation, the surface must be considered rough and it will produce a damping of the coherent intensity.

When the whole illuminated surface is considered, we have to consider a mean phenomenon. The mean value of height variation will vanish, leading to  $\langle \delta\phi_r \rangle = 0$ . However, the variance of the phase variation is

$$\langle (\delta\phi_r)^2 \rangle = 4\sigma_h^2 \left( \frac{2\pi}{\lambda} \right)^2 \cos^2 \theta_i, \quad (5)$$

where  $\sigma_h$  is the surface RMS (root mean square) height. In this study, we are only concerned with cases where the RMS height is comparable to or greater than the wavelength of the probe.

For a rough surface with Gaussian height distribution, the exponential term in Eq. (3) satisfies  $\langle \exp(i\delta\phi_r) \rangle = \exp(-\langle (\delta\phi_r)^2 \rangle / 2)$  [14], so that the intensity of the specular beam will be given by

$$|\langle E_r \rangle|^2 = |E_0|^2 \exp(-\langle (\delta\phi_r)^2 \rangle), \quad (6)$$

where  $|E_0|^2$  corresponds to the intensity reflected by a perfectly flat surface and the term  $\exp(-\langle (\delta\phi_r)^2 \rangle)$  describes the damping effect of roughness on the specular intensity. This equation explains the overall attenuation of the specular component: if  $p$  and  $s$  waves are attenuated in the same way, there will be no effect of roughness in ellipsometry measurement with specular light, but if they are attenuated in different ways there will be a change in the polarization of reflected light.

Ellipsometry essentially analyzes at the specular angle the change of polarization of light after being reflected on a sample. For a rough surface, the total scattered  $p$  and  $s$  components of the electric field ( $E_p, E_s$ ) are related to the components of the incident field ( $E_{0p}, E_{0s}$ ) by

$$E_p = (\langle r_{pp} \rangle + s_{pp})E_{0p}, \quad (7a)$$

$$E_s = (\langle r_{ss} \rangle + s_{ss})E_{0s}, \quad (7b)$$

where  $\langle r_{ii} \rangle$  and  $s_{ij}$  are respectively the mean and fluctuating components of complex reflectance coefficients.  $\langle r_{ii} \rangle$  is responsible for the specular component of the reflection and  $s_{ij}$  for the diffuse scattering component, schematically illustrated in Fig. 2. As our ellipsometer has a very small numerical aperture we can assume that only fields reflected at a specular angle are detected. Furthermore, in the above equations, we have also assumed that the material is isotropic and the roughness is random and has the same properties in all directions along the surface, which involves that the cross-polarization coefficients are zero in both the specular and diffuse components ( $\langle r_{ij} \rangle = s_{ij} = 0$  when  $i \neq j$ ).

The ensemble average of Eqs. (7) defines the collective specular response given by  $\langle E_p \rangle = \langle r_{pp} \rangle \langle E_{0p} \rangle$  and  $\langle E_s \rangle = \langle r_{ss} \rangle \langle E_{0s} \rangle$ . As the fields from the diffuse component have random phases, their ensemble average sums up to zero ( $\langle s_{ii} \rangle = 0$ ). However, this does not mean that they have a negligible contribution to experiments. Conventional ellipsometry typically only considers the specular (non-fluctuating) fields  $\langle E_r \rangle$  and ignores all the diffuse fields. However, as shown in Eq. (2), when the roughness is high, the diffusely scattered fields can contribute significantly to the overall detected intensity and must be taken into account. To include this effect, the Stokes-Mueller formalism, which deals with second-order moments, must be used. Without this, a simple average of the fields would only take into account the mean coherent term.

Stokes parameters are linear combinations of the second moments of the fields  $\langle E_i E_j^* \rangle$ . If we assume that there is no correlation between the mean part and the fluctuating part,  $\langle s_{ii} r_{jj}^* \rangle = 0$ ,

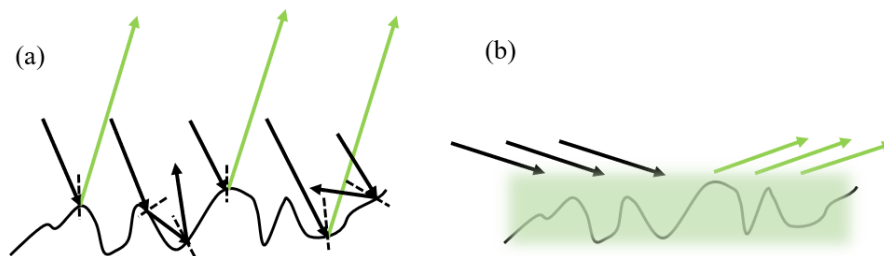


**Fig. 2.** Diffuse reflection (a) and specular reflection (b). In diffuse reflection, the detected light at specular angles comes from individual optically smooth facets, but in specular reflection, the detected light intensity and polarization are contributed by the collective effect of the surface.

the calculation of the second moments is straightforward. Each moment is calculated as

$$\langle E_i E_j^* \rangle = [\langle r_{ii} \rangle \langle r_{jj}^* \rangle + \langle s_{ii} s_{jj}^* \rangle] \langle E_{0i} E_{0j}^* \rangle. \quad (8)$$

From linear combinations of  $\langle r_{ii} \rangle \langle r_{jj}^* \rangle$  one can construct the Mueller matrix  $\mathbf{M}_{\text{spec}}$  that relates the input and output Stokes vectors corresponding to specular fields. Linear combinations of  $\langle s_{ii} s_{jj}^* \rangle$  will define the elements of the diffuse scattering Mueller matrix  $\mathbf{M}_{\text{dif}}$ . Overall, this implies that the total Mueller matrix  $\mathbf{M}$  is separated into specular and diffuse scattering contributions [12]:

$$\mathbf{M} = \mathbf{M}_{\text{spec}} + \mathbf{M}_{\text{dif}}, \quad (9)$$

For the specular component, it holds the usual definition of the ellipsometry angles  $\Psi$  and  $\Delta$ :

$$\rho_{\text{spec}} = \frac{\langle r_{pp} \rangle}{\langle r_{ss} \rangle} = \tan \Psi_{\text{spec}} \exp i\Delta_{\text{spec}}, \quad (10)$$

so that

$$\mathbf{M}_{\text{spec}} = \begin{bmatrix} 1 & -\cos 2\Psi_{\text{spec}} & 0 & 0 \\ -\cos 2\Psi_{\text{spec}} & 1 & 0 & 0 \\ 0 & 0 & \sin 2\Psi_{\text{spec}} \cos \Delta_{\text{spec}} & \sin 2\Psi_{\text{spec}} \sin \Delta_{\text{spec}} \\ 0 & 0 & -\sin 2\Psi_{\text{spec}} \sin \Delta_{\text{spec}} & \sin 2\Psi_{\text{spec}} \cos \Delta_{\text{spec}} \end{bmatrix}. \quad (11)$$

Note, however, that the complex ratio  $\rho_{\text{spec}}$  or the ellipsometry angles  $\Psi_{\text{spec}}$  and  $\Delta_{\text{spec}}$  are not equal to the ones corresponding to specular reflection on a perfectly smooth surface ( $\rho_0$ ,  $\Psi_0$  and  $\Delta_0$  respectively). Even in situations where the roughness is very small and the diffuse component can be fully neglected, it is well-known that the coherent collective effects of roughness change the polarization response of a surface [1,4], as we have previously discussed.

The diffuse component of the reflected light results from the (incoherent) superposition of waves scattered from different parts of the illuminated sample around the specular direction. If the numerical aperture is sufficiently small, one can assume that all the detected diffuse intensity comes from reflections of locally optically smooth surfaces [18,19]. In each one of these surfaces one can apply the same Fresnel equations as for a perfectly flat material, namely:

$$\rho_{\text{dif}} = \rho_0 = \tan \Psi_0 \exp i\Delta_0. \quad (12)$$

Since all these local reflections are thus characterized by the same non-depolarizing Mueller matrix, the ensemble average of the diffuse component,  $\mathbf{M}_{\text{dif}}$ , is still a non-depolarizing Mueller matrix and fully coincides with the Mueller matrix of a flat material ( $\mathbf{M}_0$ , which has the same form as Eq. (11) but using the ellipsometry angles  $\Psi_0$  and  $\Delta_0$ ). Given this coincidence, this diffuse component becomes especially interesting to measure by ellipsometry when studying very rough surfaces. For surfaces with roughness comparable to or larger than the wavelength this diffuse component can be much larger than the specular one. However, the balance between the specular and diffuse components will depend on the AOI as shown by Eq. (6), as the specular component becomes increasingly dominant at grazing angles approaching  $90^\circ$ .

For the roughness levels considered in this work (where  $\sigma_h$  is comparable or slightly larger than the wavelength), we can summarize the ellipsometry response in three main situations:

- For small AOI  $\mathbf{M} \approx \mathbf{M}_{\text{dif}} = \mathbf{M}_0$ .
- At grazing incidence (AOI close to  $90^\circ$ )  $\mathbf{M} \approx \mathbf{M}_{\text{spec}}$ .
- For intermediate AOI values both contributions should be considered, according to Eq. (9).

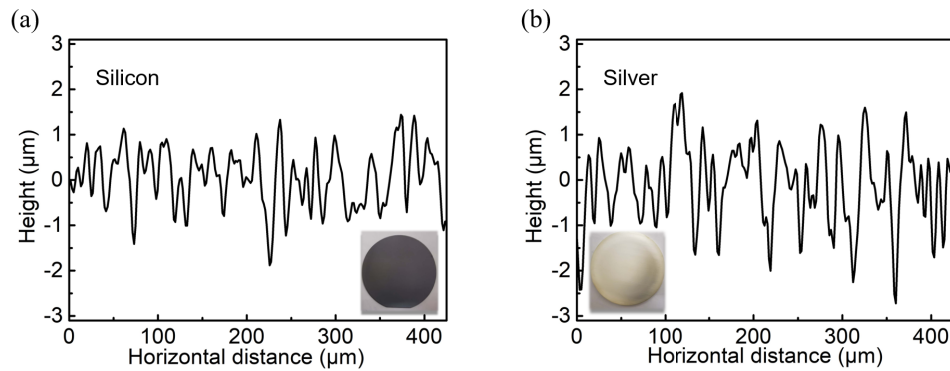


**Fig. 3.** 1D surface profile for the silicon wafer (a), and the silver sample (b). Photos of the samples are also included as inset images.

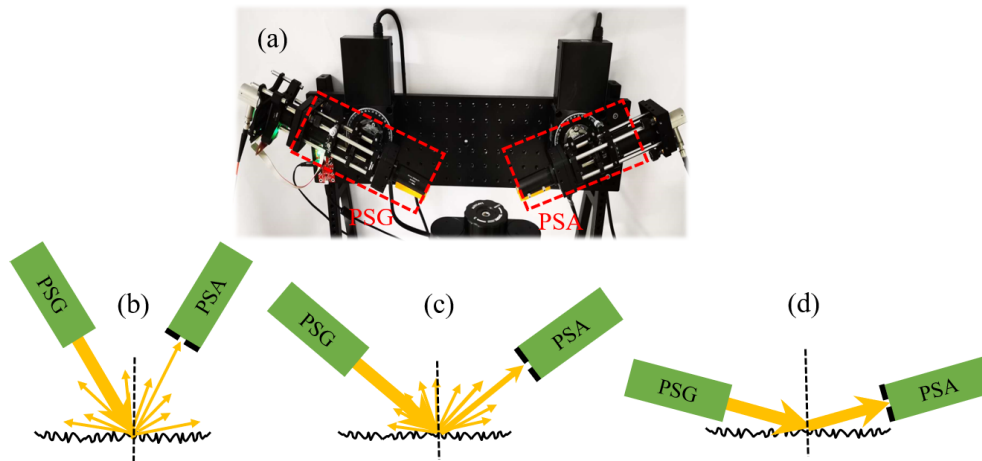


**Fig. 4.** Photo of the instrument (a) and schematic of the measurement at different AOIs (b)(c)(d). The rough sample is positioned horizontally on a holder between the PSG and PSA arms, which are arranged symmetrically. The PSA arm only collects light that is reflected in the specular direction with respect to the incident beam. To reduce the aperture of the detection, an aperture diaphragm is placed before the final parabolic mirror in the PSA arm. Schemes (b), (c), (d) emphasize the appearance of the specular reflection at grazing incidence.

Equation (9) describes the superposition of two distinct non-depolarizing Mueller matrices, both of which possess the same block-diagonal symmetry. This combination can potentially result in a depolarizing Mueller matrix. However, as demonstrated by our measurements, no measurable depolarization was detected (regardless of the AOI) within the noise level of the detection. This is due to the fact that even though  $\mathbf{M}_{\text{spec}}$  and  $\mathbf{M}_{\text{dif}}$  are different, they are relatively similar numerically, resulting in negligible depolarization.

### 3. Experiment

The studied samples in this work are the non-polished side of a (001) silicon wafer and a bare silver sputtering target (Kurt J. Lesker, 99,9% purity). In order to evaluate the roughness of the surfaces the samples were measured with an optical surface profilometer (Sensofar PLu 2300 confocal microscope). A representative example of the obtained topographies is shown in the

one-dimensional roughness profiles in Fig. 3. Optical profilometry results show that surface roughness in these samples follows a random Gaussian distribution and the obtained and the obtained height of root mean standard  $\sigma_h$  is  $0.6 \pm 0.1 \mu\text{m}$  for the Si sample and  $1.0 \pm 0.1 \mu\text{m}$  for the Ag sample. Note that these roughness values are much larger than those typically appearing in ellipsometry literature, where most usually roughness is no larger than a few nanometers.

Spectroscopic ellipsometry was performed using a custom-built Mueller matrix ellipsometer that incorporated dual Fresnel rhombs compensators with a discrete rotation implementation [20,21]. The main advantage of this instrument is that it allows for the integration time at the CCD spectrometer to be set to large values, as it is not affected by the compensator rotation

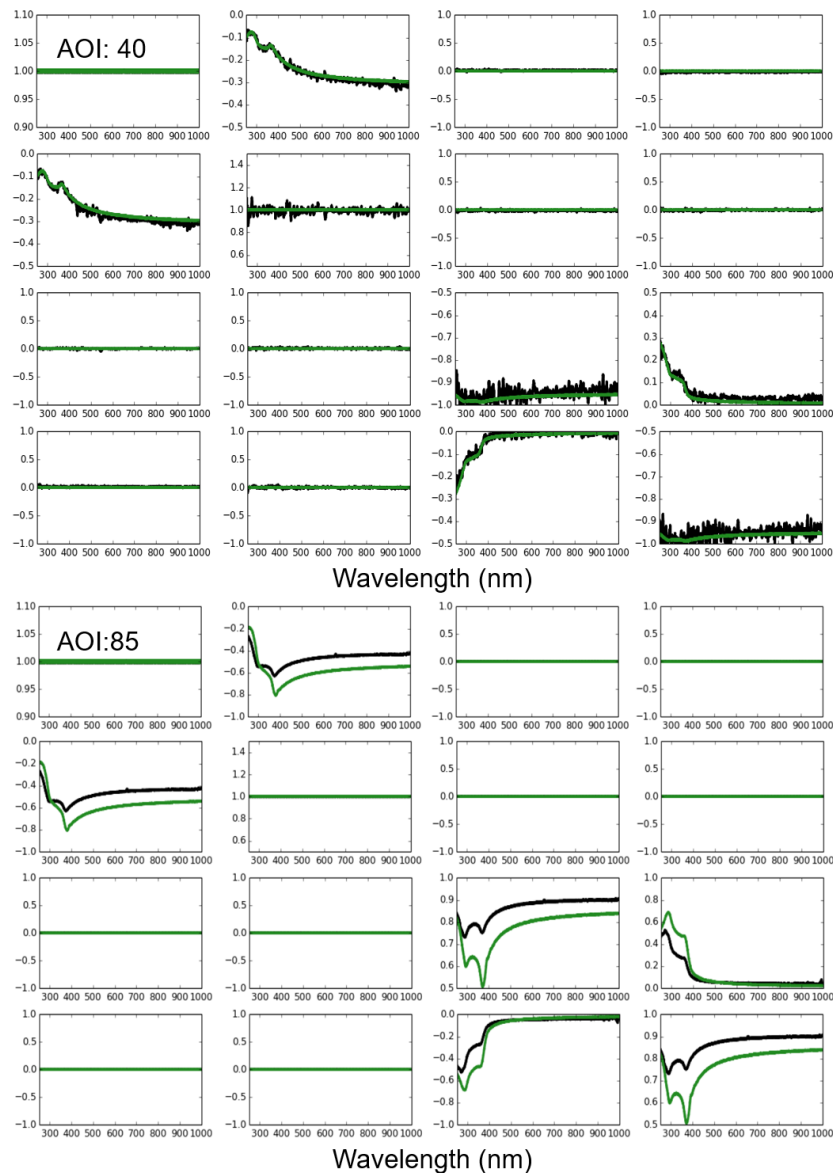


**Fig. 5.** Measured Mueller matrix of silicon rough surface (black curve) and flat surface (green curve) at AOI of  $40^\circ$  and  $85^\circ$  over the wavelength from 250 nm to 1000 nm.

speed. A photo of the instrument is shown in Fig. 4. The polarization state generator (PSG) and polarization state analyzer (PSA) arms are symmetrical with respect to the plane of the sample, allowing for the collection of light reflected at specular angles to the direction of the incident light. An additional aperture diaphragm is placed in front of the final parabolic mirror that focuses light onto an optical fiber, reducing the numerical aperture of the detection system (estimated to be below 0.002). This ensures that only light at specular angles is collected and other angles are blocked. Despite the generally weak light intensity during measurements, a significant intensity was measured by adjusting the integration time (in the measurements reported here, the integration time for each intensity acquisition varied between 20 ms to 2 s, depending on the sample and AOI used). As the PSG and PSA arms are mounted on a rotation motor, the AOI can be adjusted between a minimum of 40° and a maximum of 85°. At the smallest AOI, only diffuse light was measured and there was no specular reflection as shown in Fig. 4(b). Due to the low intensities at the detector, longer integration times were required for this configuration. As the AOI increased, the measured intensity became larger as the specular reflection appeared, as seen in Fig. 4(c). At grazing incidence, the measured intensity reached its maximum level and the contribution from diffuse light became negligible, as shown in Fig. 4(d).

Figure 5 illustrates representative Mueller matrix measurements at AOIs of 40° and 85° for the non-polished side of a silicon wafer. Measurements at other AOIs can be found in [Supplement 1](#). For comparison, the measurements made on the polished side of the silicon wafer are also shown in the figure. It is evident that the measurements on both the flat and rough sides adhere to the symmetry of Eq. (11), and no measurable depolarization is observed. Azimuthal rotation of the samples did not change the measured Mueller matrices or the observed scattering patterns, which is a result consistent with the isotropic character of the materials studied and a random roughness with the same properties in all directions. At an AOI of 40°, the Mueller matrix of the rough side (black curve) and flat side (green curve) are nearly identical across the entire spectral range despite the measurements on the rough surface being much noisier due to the low light levels. This can be attributed to the geometrical optical approximation, where only light reflected from locally approximately flat facets can enter the detector, as explained in the previous section. However, as the AOI increases, specular reflection emerges, and the rough and flat Mueller matrices gradually diverge. At the AOI of 85°, there is a clear distinction between the flat and rough measurements. The experiment on a silver sample yielded similar results, as shown in [Supplement 1](#).

#### 4. Results and discussion

Our experimental results are analyzed with the linear superposition model presented in Eq. (9) which suggests that every measured Mueller matrix can be understood as a linear combination between diffuse and specular components. As this linear combination will depend on the wavelength and the AOI, we can make these dependencies explicit and rewrite Eq. (9) as

$$\mathbf{M}(\theta, \lambda) = a(\theta, \lambda)\mathbf{M}_{\text{dif}}(\theta, \lambda) + (1 - a(\theta, \lambda))\mathbf{M}_{\text{spec}}(\theta, \lambda), \quad (13)$$

where  $a$  represents the weight ratio between the diffuse and specular components.  $\mathbf{M}$ ,  $\mathbf{M}_{\text{dif}}$ , and  $\mathbf{M}_{\text{spec}}$  are normalized Mueller matrices. As we have discussed in Section 2 and verified experimentally in the previous section, the diffuse component  $\mathbf{M}_{\text{dif}}$  (which dominates at small angles of incidence) fully coincides with the perfectly smooth surface response using the optical constants of Si or Ag. For the Si sample, we incorporated a SiO<sub>2</sub> overlayer with a thickness of 2.63 nm, which is the same value as that of the flat side, to consider the presence of the native oxide layer. On the other hand, for the Ag sample, we performed a direct fit of the diffuse term using the optical constants of Ag [22], without the need to consider any additional overlayer.

The next step is to understand the specular term  $\mathbf{M}_{\text{spec}}$ , which is less straightforward than the diffuse term. To study it, we focus on the measurements taken at an AOI of 85°. At this grazing

angle, we assume that the specular fields are much more intense than the diffuse ones, and in a good approximation, Eq. (13) is only contributed by  $\mathbf{M}_{\text{spec}}$  (i.e.,  $\mathbf{M} \approx \mathbf{M}_{\text{spec}}$ ). To study the effect that a rough surface has on the specular component  $\mathbf{M}_{\text{spec}}$ , we need to construct a suitable ellipsometry model that fits our grazing angle measurements. Once this model is available, it will be possible to calculate the Mueller matrix for specular reflection at other AOIs, so that both terms in Eq. (13) would be known.

In an initial test, we attempted to use the widely-used method of modeling roughness as an EMA Bruggeman overlayer. However, the roughness scale of our samples significantly exceeded the limits of the EMA model, resulting in a failed fit even when several EMA layers with different ratios and fractions are utilized [23]. Therefore, we developed a new phenomenological model in which the roughness is still represented as an overlayer on an otherwise flat material (the oxide layer was disregarded in the fits of  $\mathbf{M}_{\text{spec}}$  to keep the model as simple as possible since it did not substantially improve the fit results). The effect of this overlayer that accounts for the roughness is essentially attenuating or extinguishing light differently for  $p$  and  $s$  polarizations, meaning the attenuation described in Eq. (6) is not the same for  $p$  and  $s$  waves. This can occur due to the effect of the steep slopes of the roughness and shadowing effects (see Fig. 1), in which the shadowed parts of the surface may not contribute or contribute differently to the scattered field [24]. Numerical studies have shown that at grazing incidence,  $p$  polarization (i.e. incoming polarization close to perpendicular to the surface) induces much stronger surface currents in shadowed regions than  $s$  polarization (i.e. parallel to the surface) [25].

The extinction overlay can be created by setting its refractive index to match the input medium (such as  $n = 1$  for air) and its absorption coefficient to a non-zero value ( $k \neq 0$ ). This allows for the differential extinction between  $p$  and  $s$  to disappear as  $k$  approaches 0 or the thickness of the overlay,  $d$ , approaches 0, resulting in a flat material. It is important to note that the optical properties of this overlay do not represent any actual material, but instead, represent the collective effect that roughness has on the polarization of specular reflection. Additionally, the thickness  $d$  obtained from the fit is not directly related to the roughness size, as the bulk extinction effect of the overlay will scale as  $\sim kd$ . In our fits at  $85^\circ$  AOI, we only allow  $k$  to change with wavelength, parameterizing this dependence as an exponential function.

$$k = Ae^{B(E_\lambda - E_b)}, \quad (14)$$

where  $A$  and  $B$  are the two parameters, along with  $d$ , that are included in the fitting process.  $E_\lambda$  is energy corresponding to incident wavelength and  $E_b$  was fixed to 3.1 eV. This exponential function is often utilized to describe the shape of Urbach tails. After determining the values of  $k$  and  $d$  from the fit of measurements at  $85^\circ$  AOI, we can use the same stacked model to calculate the value of  $\mathbf{M}_{\text{spec}}$  at any AOI. Once the values of  $\mathbf{M}_{\text{spec}}(\theta, \lambda)$  and  $\mathbf{M}_{\text{dif}}(\theta, \lambda)$  are known, Eq. (13) can be used to analyze measurements obtained at any AOI. The weight ratio  $a$ , which determines the balance between specular and diffuse reflection, is the only free parameter that needs to be determined.

#### 4.1. Silicon

Figure 6 shows experimental results in terms of  $\Psi$  and  $\Delta$  for rough silicon measured at  $85^\circ$ , along with the best-fit values and the fitted  $k$  values of the overlay. The optical constants of silicon from [26] were used as the substrate material. The values of the two parameters that define the extinction of the overlay (Eq. (14)) obtained from the fit were  $A = 0.0387$  and  $B = -0.319 \text{ eV}^{-1}$ , and the thickness of this attenuation layer was determined to be 90.63 nm. The proposed phenomenological model can fit the experimental data from the rough wafer well. The values of  $k$  increase with wavelength because the phase variation is an inverse function of wavelength, meaning that as wavelength increases, larger portions of the rough surface contribute to the

specular reflection. Once all the parameters of the substrate and overlay are known, one can calculate  $M_{\text{spec}}$  at other AOIs.

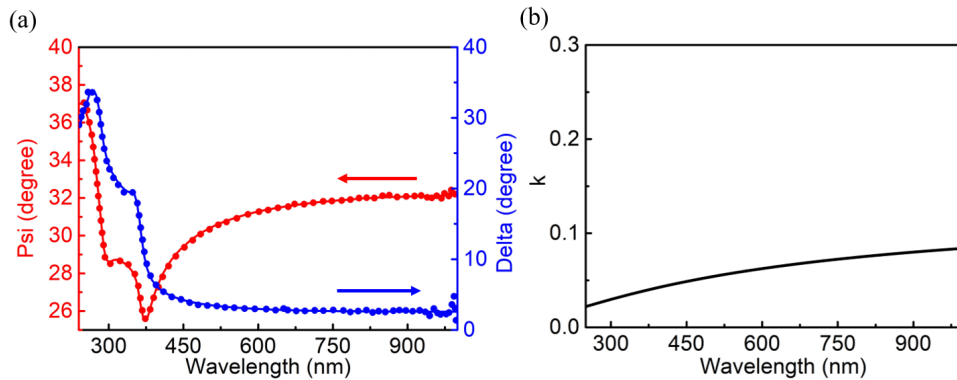


**Fig. 6.** Fits of  $\Psi$  and  $\Delta$  (b) at AOI of  $85^\circ$  for the rough silicon sample. (a) experimental points (solid circles) and simulated data (line) show good agreement over the wavelengths from 250nm-1000nm. The  $k$  values of the overlayer are shown in (b).

Using Eq. (13), it is possible to fit the Mueller matrices  $\mathbf{M}$  measured at any angle of incidence by superimposing the diffuse and specular responses. The only free parameter,  $a$ , varies with wavelength. Therefore, we first performed a wavelength-by-wavelength analysis to determine the evolution of  $a$ . The results showed that  $a$  followed a linear relation with wavelength. Therefore, we implemented a global fit for our spectroscopically measured data, where  $a$  was parameterized as a linear function of wavelength, such as  $a = m\lambda + n$ . For clarity, we only display in Fig. 7 the experimental data and the fitting results of  $\Psi$  and  $\Delta$  obtained at AOIs between  $45^\circ$  and  $70^\circ$ . Our analysis was limited to the linear dispersion relation for  $a$  that we empirically determined, but further research would be interesting to understand the relationship between  $a$  and the roughness parameters, especially in our experimental conditions where we used large angles of incidence [27]. The results of classic works on the Beckmann-Kirchoff theory [16,28] are not directly applicable to our measurements since they assume near-normal incidence.

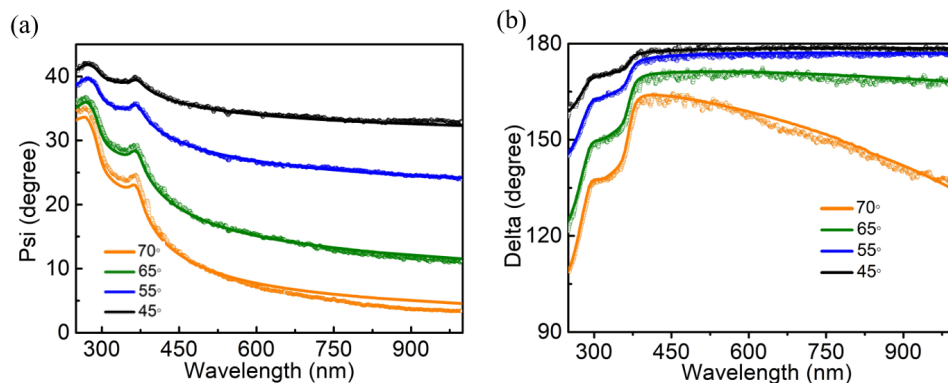


**Fig. 7.** Fitting results of  $\Psi$  (a) and  $\Delta$  (b) of the rough silicon sample at AOIs from  $45^\circ$  to  $70^\circ$ . Experimental data (circles) and simulated data (lines) are plotted together.

#### 4.2. Silver

Figure 8 illustrates the results of measuring a rough silver sample at an AOI of  $85^\circ$ . The fit used the optical constants of silver reported in a previous study [22], and included an extinction overlay with a thickness of 41.4 nm and a  $k$  defined by the parameters  $A = 0.056$  and  $B = -0.701 \text{ eV}^{-1}$ . The results show that at this AOI, the dispersion in  $k$  is similar to that of silicon, as shown in Fig. 6(b), but with larger values due to the rougher surface of the silver sample.

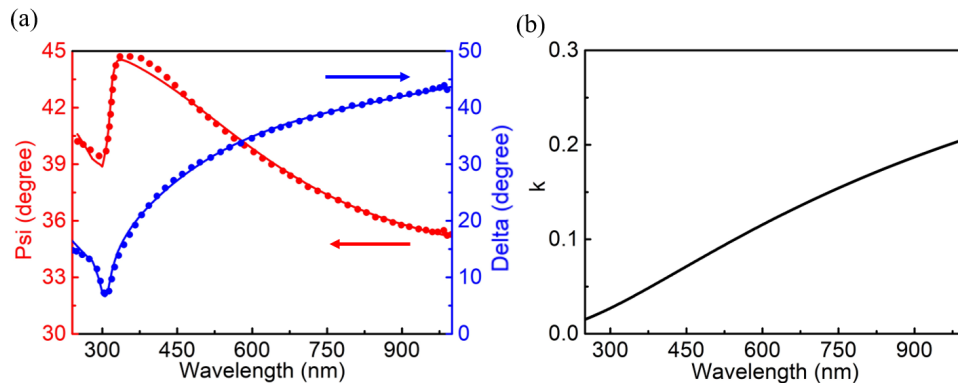


**Fig. 8.** Fits of  $\Psi$  and  $\Delta$  at  $85^\circ$  AOI for the silver sample (a). Experimental points (solid circles) and simulated data (line) show good agreement over the wavelengths from 250nm-1000nm. The  $k$  values of the overlayer are shown in (b).

Furthermore, at AOIs of  $40^\circ$  and  $45^\circ$ , the experimental data agree well with a smooth surface semi-infinite model using the optical constants reported in [22]. This indicates that within this range of AOI, the approximation of reflection by locally flat facets is fully applicable, and the measured data matches what would be measured in a flat silver sample.

Figure 9 shows the fitting results of  $\Psi$  and  $\Delta$  at AOIs from  $45^\circ$  to  $75^\circ$ . Equation (13) was used to fit all these intermediate AOIs. As in the case of silicon, a linear dispersion function for  $a$  was used.

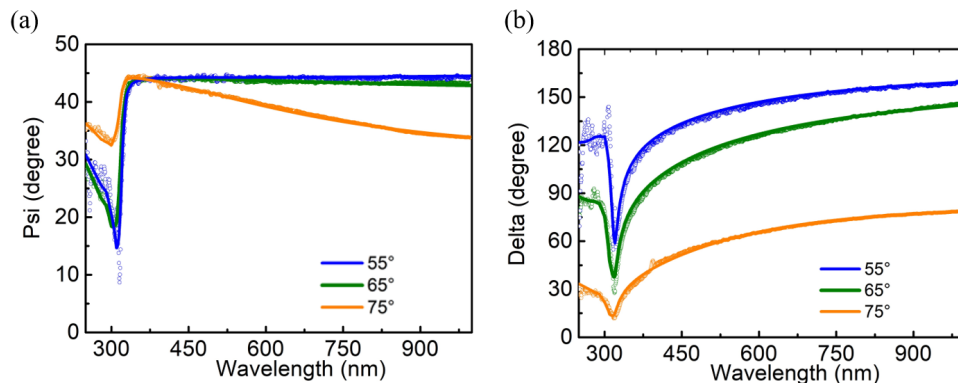


**Fig. 9.** Fitting results of  $\Psi$  (a) and  $\Delta$  (b) of the rough silver sample at AOIs from  $55^\circ$  to  $75^\circ$ . Experimental data (circles) and simulated data (lines) are plotted together.

Figure 10 presents a summary of the values of  $a$  obtained for both silicon and silver samples from the fits shown in Figs. 7 and 9. As expected,  $a$  decreases as the AOI increases. This is because  $a$  specifies the balance between diffuse and specular reflection in Eq. (13) ( $a = 1$

indicates a fully diffusive character and  $a = 0$  complete specularity). Additionally, for each AOI, there is a linear decrease in  $a$  values with wavelength, which also aligns with the expectation of the Rayleigh criterion.

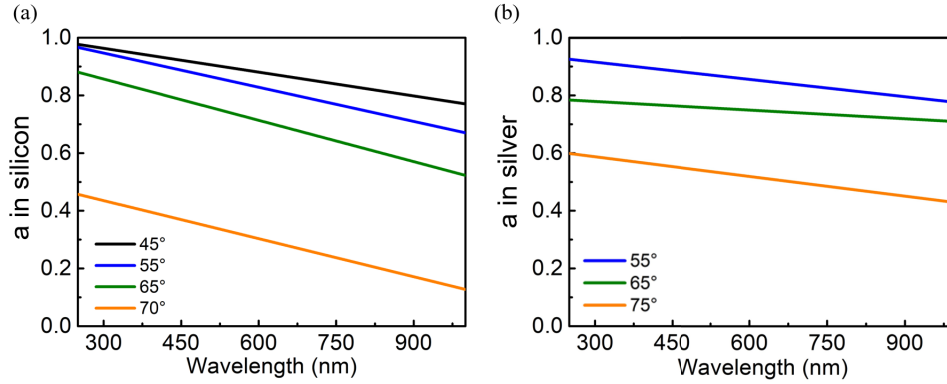


**Fig. 10.** Values of  $a$  at different AOIs for silicon (a) and silver (b). A linear dependence of the spectral response of  $a$  has been assumed.

All spectroscopic ellipsometry measurements on the rough samples of silicon and silver could be reasonably well understood using the linear combination model of Eq. (13). Table 1 lists the reduced  $\chi^2$  merit function obtained for all measurements, together with the type of contribution (diffuse, specular, or combination of both) that is applicable at each AOIs. The value of  $a$  at 550 nm for each measurement is also included for illustration. In the silicon sample, the flat-like ellipsometry response ( $a = 1$ ) given by fully diffuse scattered light is obtained until an AOI  $\sim 40^\circ$ , while in the silver sample, thanks to its larger roughness, it can be used until and AOI  $\sim 45^\circ$ . Above these values of the AOI, the effect of the specular beam can no longer be neglected.

**Table 1. Summary of fits for the experimental datasets of silicon and silver at different AOIs.**

Silicon				Silver			
AOI	$\chi^2$	Type	$a@550nm$	AOI	$\chi^2$	Type	$a@550nm$
40°	2.46	$M_{dif}$	$a = 1$	40°	3.11	$M_{dif}$	$a = 1$
45°	1.26	$M_{dif}&M_{spec}$	$a = 0.89$	45°	3.88	$M_{dif}$	$a = 1$
55°	2.85	$M_{dif}&M_{spec}$	$a = 0.85$	55°	4.50	$M_{dif}&M_{spec}$	$a = 0.87$
65°	7.13	$M_{dif}&M_{spec}$	$a = 0.74$	65°	1.63	$M_{dif}&M_{spec}$	$a = 0.76$
70°	8.85	$M_{dif}&M_{spec}$	$a = 0.34$	75°	5.90	$M_{dif}&M_{spec}$	$a = 0.53$
85°	3.36	$M_{spec}$	$a = 0$	85°	3.67	$M_{spec}$	$a = 0$

## 5. Conclusion

Experimental evidence has been presented on the feasibility of using spectroscopic ellipsometry to study extremely rough surfaces where the roughness is on par with or larger than the wavelength of light. Simple models and analysis tools have been provided to aid in understanding these measurements, highlighting the importance of considering the phase change caused by the distribution of surface irregularity heights at the position of the detector (which in ellipsometry is always at a specular angle relative to the incidence).

In ellipsometry of very rough surfaces, when the AOI is small, the individual facets that make up a rough surface behave as independent plane reflectors. As the detection arm is at a specular

angle, only locally flat facets are sampled, resulting in an ensemble average that aligns with a perfectly smooth material as predicted by the Fresnel equations. In this case, data analysis is straightforward, but the measurement can be experimentally challenging due to low detected light levels as the detector only captures a small portion of the overall diffuse light. This requires a small numerical aperture to ensure that only individual flat facets contribute to the measurement. As the AOI or wavelength increases, the amount of light detected at the detector also increases because, in addition to the diffuse light, the coherent (specular) reflection appears. This is because light reflected from facets that are not too distinct can be effectively in phase, as inferred from the Rayleigh roughness criterion. At grazing incidence, when  $\theta_i \rightarrow 90^\circ$ , nearly all of the reflected radiation is coherent, as a condition of nearly constructive interference can exist over the entire illuminated surface. This offers the highest intensity levels at the detector, as the whole rough surface collectively contributes to the specular reflection, and the contribution of diffuse light can be ignored.

We have shown that the polarization of the specular beam reflected from a rough surface no longer aligns with the polarization of a perfectly flat surface predicted by the Fresnel equations. This is due to the small phase differences created by surface irregularities, in addition to other factors such as shadowing, which can subtly alter the polarization of the specular beam. To understand these changes in polarization, it is possible to modify the Fresnel equations of a flat substrate with an effective overlayer that incorporates the collective effect of surface roughness on the polarization of the specular beam. For the extremely rough surfaces we have measured, we have determined empirically that this can be achieved through the use of an extinction overlayer, characterized by a specific extinction coefficient  $k$  and thickness. We were able to analyze cases where both specular and diffuse reflectances have a significant contribution to the overall intensity through the linear superposition of two Mueller matrices. This simple model is adequate to explain the results at any AOI and across any spectral range.

With appropriate instrumentation, the characterization of very rough surfaces with spectroscopic ellipsometry is not significantly more complex than for surfaces with roughness much smaller than the probing wavelength. In fact, in some experimental configurations with small AOI, when there is no specular beam, it can even be simpler because the roughness effect becomes negligible and the inversion of the ellipsometry equation using Fresnel equations is straightforward. Our findings demonstrate that the technique of spectroscopic ellipsometry can be extended to the study of rough surfaces without the need for further processing, thus enabling the measurement of the optical constants of materials with rough surfaces.

**Funding.** Ministerio de Ciencia, Innovación y Universidades (RYC2018-024997-I, TED2021-129639B-I00); National Natural Science Foundation of China (52275531); China Scholarship Council (202108350066).

**Disclosures.** The authors declare no conflicts of interest.

**Data availability.** Data underlying the results presented in this paper are available upon request.

**Supplemental document.** See [Supplement 1](#) for supporting content.

## References

1. C. A. Fenstermaker and F. L. McCrackin, "Errors arising from surface roughness in ellipsometric measurement of the refractive index of a surface," *Surf. Sci.* **16**, 85–96 (1969).
2. D. Franta and I. Ohlídal, "Comparison of effective medium approximation and Rayleigh–Rice theory concerning ellipsometric characterization of rough surfaces," *Opt. Commun.* **248**(4-6), 459–467 (2005).
3. D. Aspnes, J. Theeten, and F. Hottier, "Investigation of effective-medium models of microscopic surface roughness by spectroscopic ellipsometry," *Phys. Rev. B* **20**(8), 3292–3302 (1979).
4. D. Aspnes, "Optical response of microscopically rough surfaces," *Phys. Rev. B* **41**(15), 10334–10343 (1990).
5. S. Fang, W. Chen, T. Yamanaka, and C. Helms, "Comparison of Si surface roughness measured by atomic force microscopy and ellipsometry," *Appl. Phys. Lett.* **68**(20), 2837–2839 (1996).
6. W. Yu, C. Cui, H. Li, S. Bian, and X. Chen, "FDTD-based study on equivalent medium approximation model of surface roughness for thin films characterization using spectroscopic ellipsometry," *Photonics* **9**(9), 621 (2022).
7. S. H. Westin, J. R. Arvo, and K. E. Torrance, "Predicting reflectance functions from complex surfaces," *ACM Siggraph Comput. Graph.* **26**(2), 255–264 (1992).

8. T. A. Germer, "Full four-dimensional and reciprocal Mueller matrix bidirectional reflectance distribution function of sintered polytetrafluoroethylene," *Appl. Opt.* **56**(33), 9333–9340 (2017).
9. T. A. Germer and C. C. Asmail, "Goniometric optical scatter instrument for bidirectional reflectance distribution function measurements with out-of-plane and polarimetry capabilities," in *Scattering and Surface Roughness*, vol. 3141 (SPIE, 1997), pp. 220–231.
10. T. A. Germer, "Modeled integrated scattering tool (mist)," National Institute of Standards and Technology, Gaithersburg, Maryland **20899**, 1 (2017).
11. N. C. Bruce, O. G. Rodríguez-Herrera, C. N. Ramírez, and M. Rosete-Aguilar, "Rough surface scattering using a source able to produce an incident beam with controlled polarization and coherence," *Appl. Opt.* **60**(5), 1182–1190 (2021).
12. S.-M. F. Nee, "Polarization of specular reflection and near-specular scattering by a rough surface," *Appl. Opt.* **35**(19), 3570–3582 (1996).
13. L. Rayleigh, "On the dynamical theory of gratings," *Proc. R. Soc. Lond. A* **79**(532), 399–416 (1907).
14. N. Pinel, C. Bourlier, and J. Saillard, "Degree of roughness of rough layers: Extensions of the Rayleigh roughness criterion and some applications," *Prog. Electromagn. Res. B* **19**, 41–63 (2010).
15. C. Bourlier and N. Pinel, *Electromagnetic wave scattering from random rough surfaces: Asymptotic models* (John Wiley & Sons, 2013).
16. P. Beckmann and A. Spizzichino, *The Scattering of Electromagnetic Waves from Rough Surfaces*, A Pergamon Press book (Pergamon Press; [distributed in the Western Hemisphere by Macmillan, New York], 1963).
17. J. Lekner, *Theory of reflection of electromagnetic and particle waves*, vol. 3 (Springer Science & Business Media, 1987).
18. K. Tang, R. A. Dimenna, and R. O. Buckius, "Regions of validity of the geometric optics approximation for angular scattering from very rough surfaces," *Int. J. Heat Mass Transfer* **40**(1), 49–59 (1996).
19. D. Bergström, J. Powell, and A. Kaplan, "The absorption of light by rough metal surfaces—a three-dimensional ray-tracing analysis," *J. Appl. Phys.* **103**(10), 103515 (2008).
20. S. Bian, C. Cui, and O. Arteaga, "Mueller matrix ellipsometer based on discrete-angle rotating Fresnel rhomb compensators," *Appl. Opt.* **60**(16), 4964–4971 (2021).
21. S. Bian, X. Xu, C. Cui, and O. Arteaga, "Calibration of achromatic Fresnel rhombs with an elliptical retarder model in mueller matrix ellipsometers," *Thin Solid Films* **763**, 139581 (2022).
22. H. U. Yang, J. D'Archangel, M. L. Sundheimer, E. Tucker, G. D. Boreman, and M. B. Raschke, "Optical dielectric function of silver," *Phys. Rev. B* **91**(23), 235137 (2015).
23. G. Jellison, T. Aytug, A. Lupini, M. Paranthaman, and P. Joshi, "Optical properties of a nanostructured glass-based film using spectroscopic ellipsometry," *Thin Solid Films* **617**, 38–43 (2016). European Materials Research Society Spring Meeting 2015, Symposium DD [E'MRS 2015 Symp. DD].
24. I. Ohlídal and D. Nečas, "Influence of shadowing on ellipsometric quantities of randomly rough surfaces and thin films," *J. Mod. Opt.* **55**(7), 1077–1099 (2008).
25. J. M. Sturm and J. C. West, "Numerical study of shadowing in electromagnetic scattering from rough dielectric surfaces," *IEEE Trans. Geosci. Electron.* **36**(5), 1477–1484 (1998).
26. G. Jellison Jr., "Optical functions of silicon determined by two-channel polarization modulation ellipsometry," *Opt. Mater.* **1**(1), 41–47 (1992).
27. J. Harvey, A. Krywonos, and C. L. Vernold, "Modified Beckmann-Kirchhoff scattering model for rough surfaces with large incident and scattering angles," *Opt. Eng.* **46**(7), 078002 (2007).
28. J. Porteus, "Relation between the height distribution of a rough surface and the reflectance at normal incidence," *J. Opt. Soc. Am.* **53**(12), 1394–1402 (1963).